ORIGINAL RESEARCH ARTICLE

Arsenic Condensation and Reaction Mechanisms in Flash Smelting Off-Gas Line Conditions

XINGBANG WAN, DMITRY SUKHOMLINOV, PEKKA TASKINEN, MARI LINDGREN, RADOSLAW MICHALLIK, and ARI JOKILAAKSO

Arsenic is a common impurity element in sulfide concentrates. It tends to accumulate in the flue dust of smelting furnace due to the volatility and internal circulation of the flue dust practiced in the smelting-converting process chain. The only outlets for arsenic are anodes and discard slag. Arsenic condensation in dust-free conditions was studied below 800 °C where the gas atmosphere was controlled by SO_2-air-N_2 gas mixtures. Based on these experimental results, we confirm the kinetically constrained formation mechanism of the arsenic-containing dust, and its speciation into metallic, oxidic (III, V), and sulfidic species. The influences of temperature and atmosphere on the speciation of arsenic were compared with industrial data and discussed.

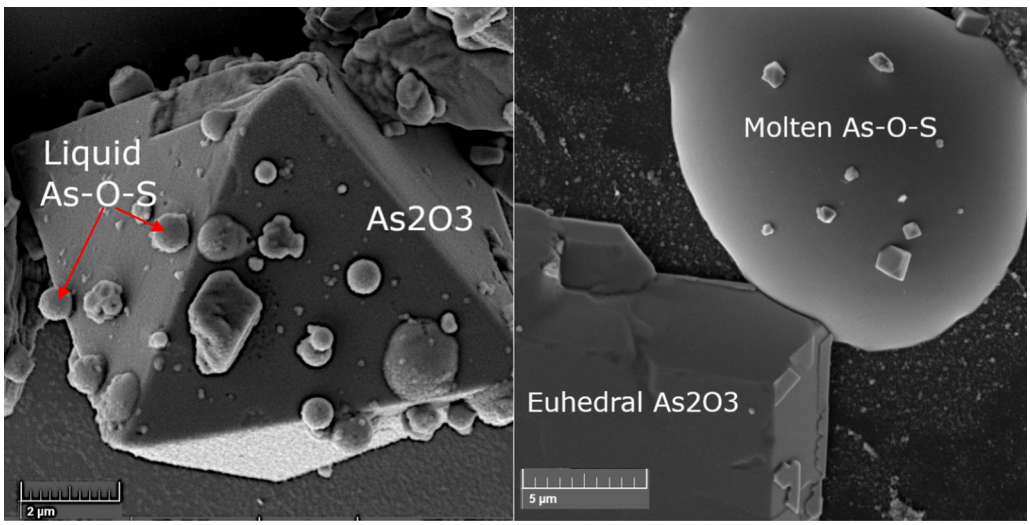

Condensed arsenic-bearing particles collected by electrophoretic forces on the surface of fused SiO_2 in SO_2-O_2 atmospheres: the crystal morphology shows euhedrally facetted As_2O_3 crystals and initially molten As-OSalloy droplets together with poorly crystallized AsS_x particles.

https://doi.org/10.1007/s11663-023-02871-9

XINGBANG WAN is with the Central South University, School of Energy Science and Engineering, Changsha, 410083, P.R. China. DMITRY SUKHOMLINOV, PEKKA TASKINEN and ARI JOKILAAKSO is with the Aalto University, School of Chemical Engineering, Department of Chemical and Metallurgical Engineering, PO Box 16100, 00076 Aalto, Finland. Contact e-mail: pekka.taskinen@aalto.fi MARI LINDGREN is with the Metso Outotec Finland Oy, Research Center, Kuparitie 10, 28330 Pori, Finland. RADOSLAW MICHALLIK is with the Geological Survey of Finland (GTK), Vuorimiehentie 2K, 02150, Espoo, Finland.

Manuscript submitted February 2, 2023; accepted July 17, 2023.
Article published online July 27, 2023.

I. INTRODUCTION

THE technology of suspension smelting is commonly used in copper, nickel, and lead sulfide smelting. Its oxidation processes between fine dry feed mixture and oxygen-enriched air in the reaction shaft of a flash smelting and converting furnace (FSF and FCF).[1,2] At the same time, the reacting particles increase their temperatures in excess to the melting point of magnetite.[3,4] This allows vaporization of many low-boiling

point impurities like arsenic into the process gas. The flue dusts from the smelting contain a fraction of the fines after suspension oxidation and gaseous elements or compounds of the oxidation products following the main off-gas stream to the settler and further to the uptake.

Typical off-gas of a FSF contains up to 50-70 vol pct SO_2 and those of an FCF are typically higher.[5] The oxygen concentration depends on how carefully the post-combustion and flue dust sulfation in the waste heat boiler (WHB) after the smelting vessel are carried out.[6] That extra oxygen should be enough to generate sulfates from sulfate forming elements.[6,7]

The quality and copper grade of copper concentrates have been on decline over decades.[8] This means that various complex concentrates containing copper and iron-bearing impurity minerals, such as arsenopyrite (FeAsS), enargite (Cu_3AsS_4), and tennantite ($Cu_{13}As_4S_{12}$), have become increasingly common in the commodity trading. Therefore, the amounts of these harmful elements in the smelting and refining circuits have increased inducing studies about arsenic and other impurities' speciation in flue dust of the gas train.[9–11] Those studies may exhibit systematic errors due to the small submicron particle size of the condensed dust, despite of using the very surface-sensitive XPS (X-ray photoelectron spectroscopy) technique in many studies. For tackling the problems, several studies have been recently published about a separate treatment of the flue dusts, for bleeding arsenic from the smelter and lowering its concentrations in the anodes and discard slag.[12–14]

In copper smelting, arsenic thermodynamically favors the matte phase[15,16] but the high vapor pressures of arsenic species and high oxygen partial pressure at the end of the converting step lead to its strong deportment in the process gas.

The high volatility of arsenic is due to the low boiling points of metallic arsenic, As_2O_3, and As_2S_3.[17,18] Thus, the volatilization and perhaps condensation depend on the prevailing atmosphere, its oxygen, and sulfur dioxide partial pressures. The high vapor pressure of pure As_2O_3 implies also that arsenic is condensed in the industrial sulfide smelter off-gas train at low temperatures, beyond the electrostatic precipitator (ESP). Practically, no focused studies about the precipitation of arsenic in typical copper smelting off-gas train condition have been published. The aim of this study is to examine in detail the arsenic deposition in conditions simulating the off-gas from the WHB temperatures to those in the acid plant-washing section, as a first approximation without flue dust. A novel experimental setup was developed for this purpose. The results are expected to help controlling/adjusting off-gas composition for better As recovery/separation in the off-gas train.

II. EXPERIMENTAL

A. *Materials and Experimental Setup*

The raw materials were pure metallic arsenic lump (Alfa Aesar, 99.999 pct pure) and silver shots (Boliden Harjavalta, 99.999 pct pure). The experimental atmosphere was achieved by mixing SO_2 (99.98 vol pct pure, Aga-Linde), air (<0.001 g/m^3 H_2O), and N_2 gases (99.999 vol pct pure, Woikoski, Finland). The gas flow rates were regulated using digital mass flow controllers DFC26 (Aalborg). Silver was selected as solvent for arsenic due to its stability against oxidation in the gas mixtures used.

The novel experimental apparatus used for the condensation study was a modified transportation setup where arsenic was vaporized freely from a molten silver-arsenic alloy at a fixed temperature to a premixed carrier gas containing O_2(g), SO_2(g), and N_2(g). Thus, the initial situation in the gas at 800 °C was similar to that in the FSF where arsenic compounds are dissociated to elemental form.[19] The industrial smelter off-gas contains dust which was not included in the present study. The selected setup design allows condensation of arsenic compounds in a controlled temperature gradient,[20] sometimes called thermochromatography.[21] The vertical design avoided settling of the homogeneously nucleated material on the fused silica riser tube, and the deposit was formed by electrophoretic forces. The lead time of the gas in the riser from the alloy surface to the outlet was estimated to be 10.5 seconds.

The setup shown in Figure 1 was designed specifically for these experiments. It comprised a vertical resistance tube furnace LHA12/300 (Lenton, UK) equipped with metal heating elements. On top of the furnace, brass flanges with a cooling water circulation were placed to hold an alumina work tube (Kyocera AL23, Germany; o.d. = 40 mm) closed in one end, and a fused silica dust-collecting tube, 'riser' (Finnish Special Glass, Finland; i.d. = 12.5 mm). A rubber plug was used to seal the silica riser on top, having a hole for inserting either a calibrated Pt100 resistance thermometer (tolerance class B 1/10 DIN) or the gas outlet tube #2. Temperature in the furnace was controlled by a Eurotherm PID controller, and the data were logged in with a LabVIEW software. The resistance of Pt100 probe was measured using a Keithley 2000 DMM digital multimeter (USA) connected to a PC for data logging (with a frequency of 0.2 1/s) during the measurements. The design allowed As additions in the furnace during the experiment without cooling.

The furnace off-gas was cleaned with hydrogen peroxide solution to oxidize the arsenic to higher valence and to reduce its toxicity, and then SO_2 was absorbed by a NaOH solution with BTS as pH indicator (bromothymol blue, $C_{27}H_{28}Br_2O_5S$, Sigma-Aldrich) before venting to the fume hood.

Two alumina crucibles were located in the bottom of the work tube in the constant temperature zone of the furnace. The larger crucible was used to insert and lift up the As source and the smaller contained the Ag-As alloy. The bottom part of the silica riser tube was placed next to the smaller crucible for better mixing the carrier gas and arsenic vapors before leading them into the vertical riser tube.

B. *Experimental Procedure*

Before the experiments, the volatile material samples were loaded in the furnace with an iron wire. In each experiment, the initial volatile material was composed of 1 g arsenic and 10 g silver. Then, nitrogen was lead through the gas inlet with a flow rate of 150 mL/min. We kept the valve #1 open and valve #2 closed when the

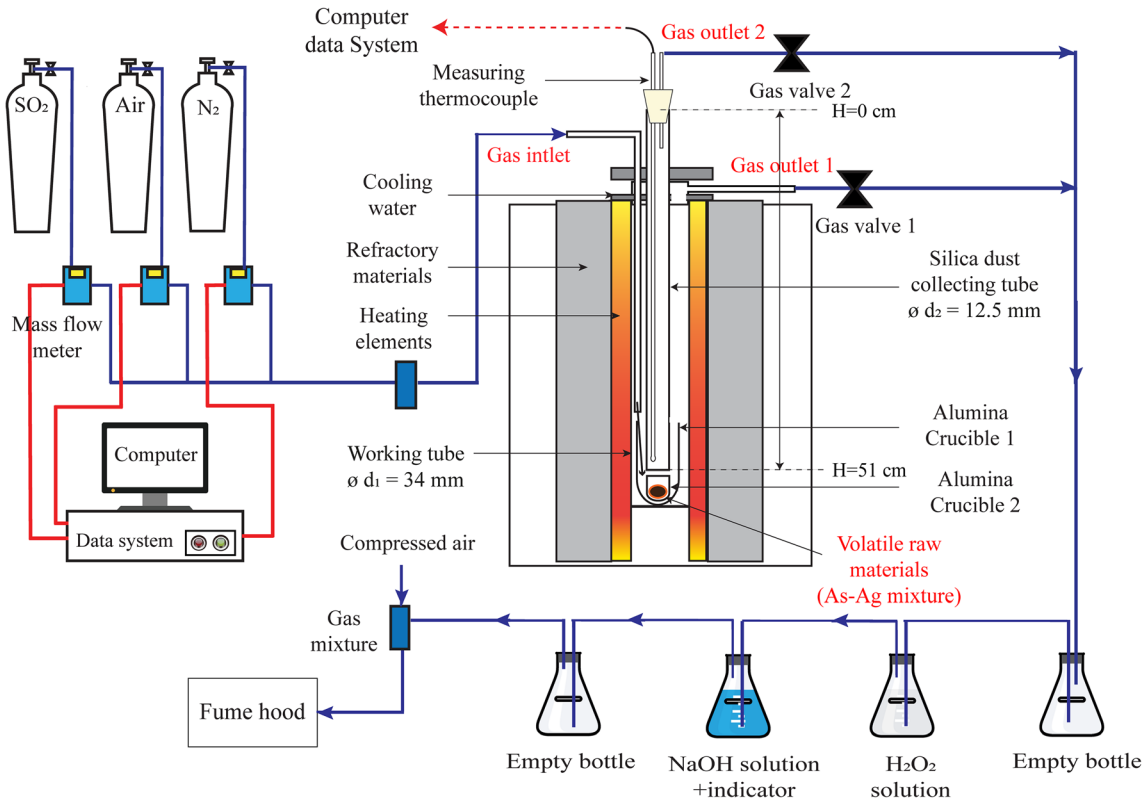

Fig. 1—Schematic of the experimental furnace, the controls, and data-logging device. Note the two off-gas lines (#1 and #2) for leading the carrier gas stream from the riser tube during heat up and cooling.

furnace temperature increased to 800 °C with the rate of 7 °C/min. After reaching 800 °C, the valve #2 was opened and valve #1 turned off, directing the gas flow through the silica riser to start the sample collection process. At the same time, the atmosphere was changed to a mixture of SO_2, air, and N_2. Dust-collecting time was 1 h in each experiment. After that, off-gas valve #2 was closed and valve #1 was turned on for nitrogen flow with a rate of 150 mL/min during cool down the furnace. Three experimental atmospheres tested in this work are shown in Table I.

Temperature of the silica riser tube at different heights varied and its temperature profile were measured before the experiments at 150 mL/min nitrogen flow, as shown in Figure 2. Thus, the specific atmosphere and temperature conditions of the collected dust samples were precisely controlled.

After the furnace reached room temperature, the silica riser was taken out from the furnace and dust in the inside wall was collected, as shown in Figure 2. The dust samples were separated from different heights of the silica tube, corresponding to the different temperature regions.

C. *Analytical Methods*

The samples were prepared with dry metallographic methods and first analyzed with a Mira 3 scanning electron microscope (SEM, Tescan, Czech Republic) equipped with an UltraDry silicon drift energy-dispersive X-ray spectrometer (EDS, Thermo Fisher Scientific, Waltham, MA) coupled to a NSS micro-analysis software (Thermo Fisher Scientific). The standards (Astimex, Canada) utilized in the EDS analyses were quartz (O Kα and Si Kα), pentlandite (S Kα), metallic silver (Ag Lα) and arsenic (As Kα).

The particle sizes were measured from the SEM pictures, the mineralogical phases and their compositions were first analyzed by EDS. To further confirm the mineralogical phases and chemical speciation, samples were investigated by X-ray diffraction (XRD), electron probe micro-analysis (EPMA), and X-ray photoelectron spectroscopy (XPS).

Due to limited amounts of the collected samples, a zero-background silicon disk was used in the XRD analysis. The samples were first ground and homogenized in an agate mortar; then an appropriate amount of ethanol was added into the mortar to form a slurry. The slurry was poured on the zero-background silicon disk and the ethanol was evaporated naturally in 10-15 mins, after which the sample was forwarded to XRD analysis. The X'Pert PRO MPO Alpha1 powder XRD (PANalytical, Netherlands) analysis used Cu Ka radiation and a scan rate of 2°/min from 10° to 90° (acceleration voltage 40 kV, current 40 mA).

The EPMA used for confirming the EDS analyses was a Cameca SX100 (France) equipped with five wavelength dispersive spectrometers. The samples were repolished using water-based suspension. The accelerating voltage used was 20 kV, beam current 10 nA, and beam diameter 5 and 10 μm. The analyzed characteristic

Table I. The Gas Component Flow Rates at Different Target Atmospheres

Target Gas Compositions (Vol Pct)	Total Gas Flow (mL/min)	SO_2 (mL/min)	Air (mL/min)	N_2 (mL/min)
50 pct SO_2 -49.5 pct N_2-0.5 pct O_2	150	75	3.6	71.4
50 pct SO_2 -48.0 pct N_2-2 pct O_2	150	75	14.4	60.6
50 pct SO_2 - 45.0 pct N_2-5 pct O_2	150	75	36.0	39.0

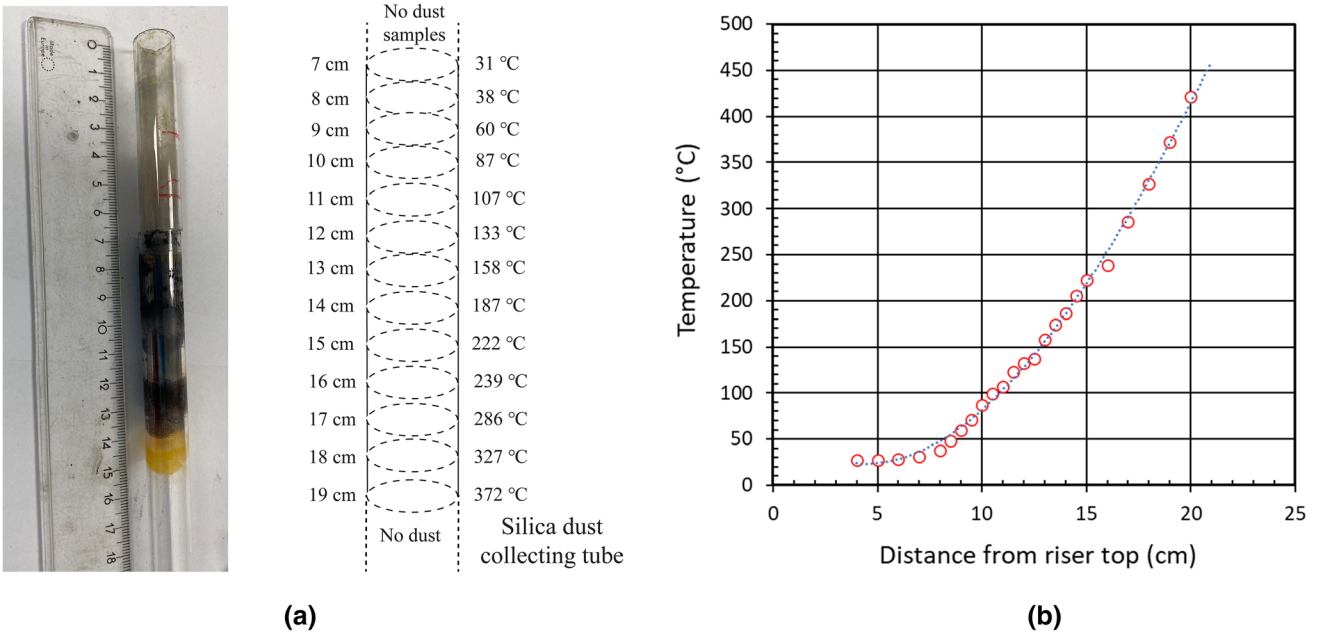

Fig. 2—Silica riser tube sections used for collecting the deposits (*a*) and the temperature profile at a constant furnace temperature of 800 °C (*b*), with a total gas flow rate of 150 mL N_2/min.

X-ray lines and external standards (Astimex) used were S Kα (sphalerite), O Kα (obsidian), Ag Lα (Ag), and As Kα (cobaltite). The average detection limits were 300 ppmw, 940 ppmw, 1040 ppmw, and 120 ppmw for Ag, As, O, and S, respectively.

The XPS spectra were recorded using a Kratos Axis Ultra spectrometer at 45 W power (instead of typical 200 W[22]) and Al anode (1486.7 eV) using exposure times of 1, 5, and 10 minutes. The measurements were performed with a 20 keV pass energy and 0.1 eV energy step. Survey spectra and the high-resolution (HR) spectra of As 3d, O 1s, S 2p, Ag 3d, and C 1s regions for selected 13 samples from the experimental series were measured. The instrument has been calibrated (a two-point calibration) using Au 4f and Ag 3d peaks. For each measurement/sample, a one-point energy correction was made where the binding energy (B.E.) of C 1s was set to a reference value (285.0 eV). The peak fitting was performed with the CasaXPS software.[23]

The speciation of arsenic was estimated from the As 3d peaks, combined with information collected from the S 2p peaks. It could be observed that the XPS data obtained from the deposits generated at the lowest oxygen partial pressure ($p(O_2)$ = 0.5 vol pct) were not stable from one electron radiation exposure time to another. Moreover, due to the very low concentration of silver in the deposits, its HR spectra exhibited a low S:N ratio.

The fitting included base line approximation by Shirley extrapolation. The HR peak shapes were fitted with *gmix* values of 0.6 for metal and 0.3 for non-metal peaks.[24] The speciation of arsenic included metallic component (As° with B.E of 41.4 eV), trivalent oxide component (As(III-O) with B.E. of 44.9 eV), pentavalent oxide component (As(V-O) with B.E. of 45.8 eV), and sulfidic components (As(III-S), orpiment (with B.E. of 43.5 eV) and As(II-S), and realgar (with B.E. of 43.4 eV).[22,25,26] The HR spectrum of sulfur was fitted using the peak of sulfur in orpiment and realgar with B.E. of 161.05 eV,[26] elemental sulfur with B.E of 164.1 eV, and +6-valent sulfur (sulfate) with B.E. of 168.0 eV.[26–28] Some fitting results are shown numerically in Table S-4 in electronic supplementary file.

III. RESULTS

Thermodynamic equilibrium calculations show that in the present conditions resembling the off-gas train of a sulfide smelter, As_2O_5 is the predominant solid oxide in the As-O system.[29] The gas phase contains a complex

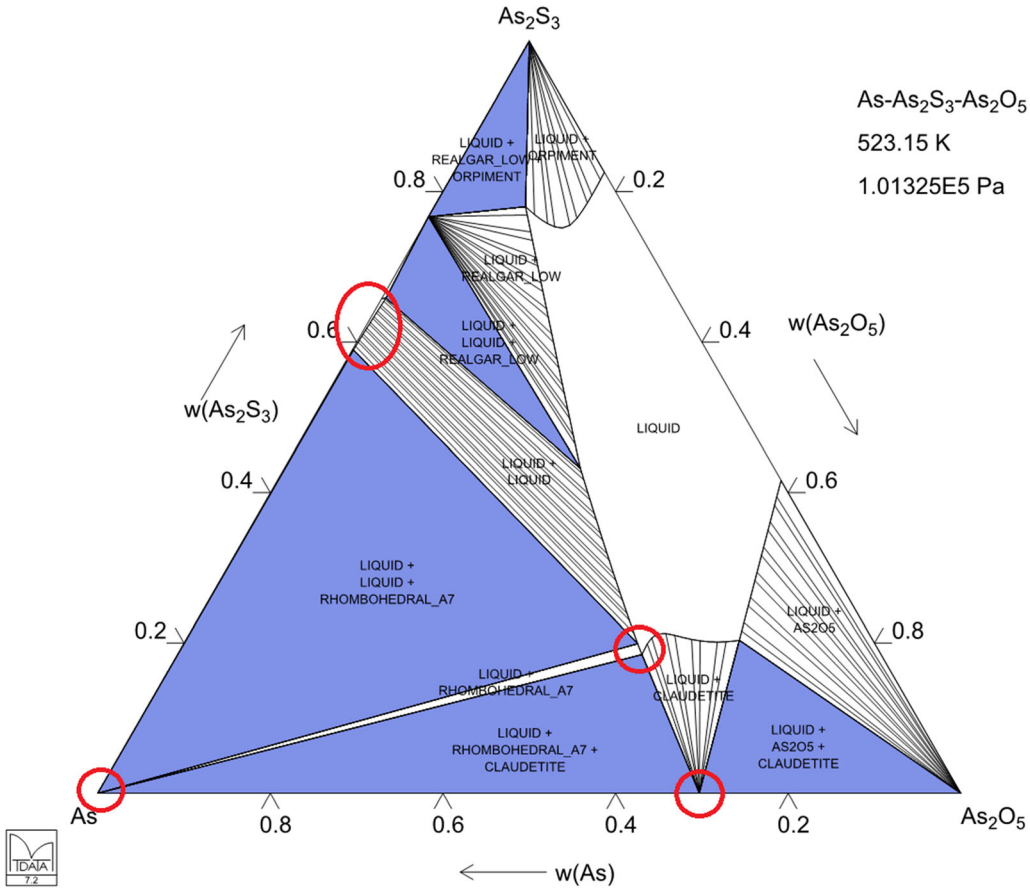

Fig. 3—An isothermal section of the As-O-S system at 1 atm, 250 °C with As, As_2O_5, and As_2S_3 as terminal phases calculated using MTOX (vers. 8.2) database using MTDTA software; red circles indicate deposit compositions found at 100-250 °C by EDS/EPMA.

combination of AsO_x and AsS_x species, but the saturated partial pressures of metallic and sulfidic arsenic species are much lower than those of arsenic oxides.[30] The ternary system As-O-S has been assessed by Gisby,[31] and the isothermal section of As-As_2S_3-As_2O_5 at 250 °C is reproduced in Figure 3. It shows several primary phase areas and one liquid immiscibility region where As-S liquid is in equilibrium with As-O-S melt; the dimer of As_2O_5(g) is the prevailing arsenic oxide species in the equilibrium gas, see Figure S-1 in electronic supplementary file.

The deposits in the riser formed at temperatures below 350 °C in all atmospheres studied with 0.5, 2, and 5 vol pct O_2 in N_2-50 vol pct SO_2 mixtures, see Table S-I in electronic supplementary file. The amount of deposit in each segment varied from 20 mg to 400 mg. The present results indicate that the deposits are far from being the equilibrium phase assemblies of the As-N_2-O_2-SO_2 systems. They contained at most temperatures one to three phases, which can be identified qualitatively based on their morphological features. No silver was found by EPMA in the deposits as expected due to its low saturated vapor pressure.[32]

Figure 4 shows selected surface morphologies of the deposits at different temperatures and oxygen volume concentrations in the input at $p(SO_2) = 0.5$ atm. The SEM micrographs show clearly that in addition to crystalline phases, molten droplets have been also generated over the entire temperature range. The phases and their compositions were identified by XRD and SEM-EDS, as well as EPMA from the polished sections.

The polished sections were prepared for analyzing the chemical compositions of the phases formed at different temperature ranges. The SEM-EDS observations show a clear pattern how the deposit has been formed in the riser. The nucleation of arsenic phases has involved significant chemical reactions between the As-bearing gas stream and its sulfur as well as oxygen species. Figure 5 shows selected cross sections in the studied atmospheres.

The EDS data show that the crystalline, euhedral phase is arsenic (III) oxide, and there is both metallic and sulfidic arsenic present at least above about 110 °C. The spheroidic shape of the metallic arsenic droplet below 200 °C, Figures 4(a), (f), indicates that As-O-S alloy has been molten at that temperature when the riser tube has been cooled down post experiment to room temperature. The stoichiometry of arsenic sulfide (AsS_x) was close to As_4S_4 (realgar) which is present with melt in the binary system down to 213 °C to 204 °C.[30,31] .However, the sulfide precipitates at the high temperature side of the deposit, as shown in Figure 4(f), seem to be close to As_2S_3 (orpiment) in their composition. The melting point of pure As_2S_3 is 313 °C.[30]

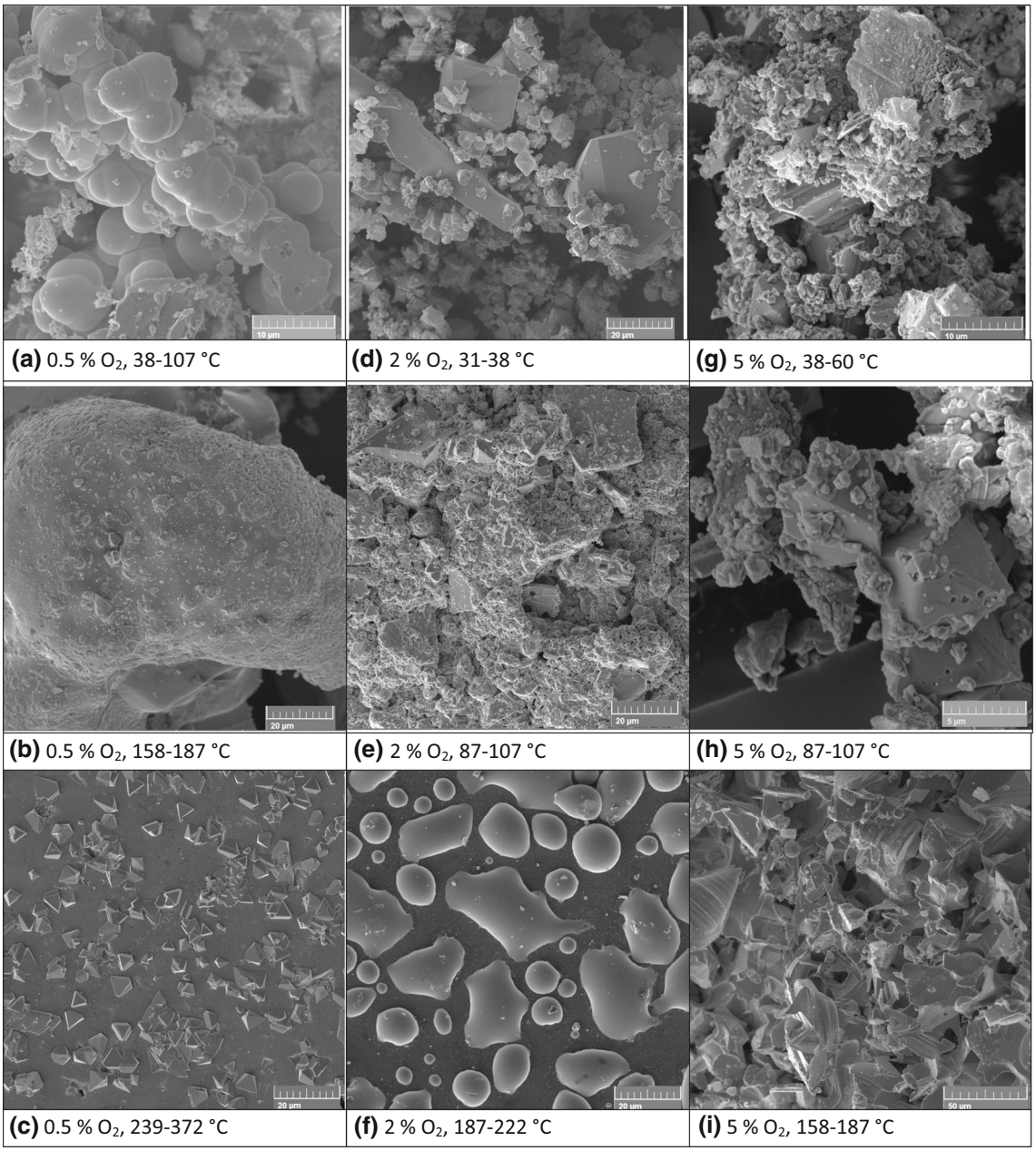

Fig. 4—Surface morphologies of As-O-S deposits formed at different temperatures and in different atmospheres.

Another example of melt formation is the discrete ponds found in 0.5 and 2 pct O_2 atmospheres at 38°C °C to 107 °C and 187°C to 222 °C, Figs. 4(a), (f) and at 107 to 158 °C and 133 to 222 °C, Figures 5(a), (b) and (e), (f). In the As-O-S system, ternary liquid is stable to lower temperatures, below 150 °C.[31] The corresponding cross sections in 2 pct O_2-50 pct SO_2 atmosphere at different temperatures are shown in Figures 5(c), (d). The gray phase in the SEM micrographs of Figure 5 shows consistently the As:O stoichiometry of As_2O_3 by EDS and EPMA observations.

In general, the low-temperature deposits (<150 °C) were showing the As-S phase domains with a low concentration of sulfur and their As:S atomic ratios were along the As-As_2S_3 joint of the system. The approximate composition of the forming deposit system based on the EDS data of the present study is shown as red circles in Figure 3. In addition to the pure sulfide and metal phase areas, some liquid As precipitates at 133 °C to 158 °C had thin scales on them indicating oxidation by the surrounding atmosphere. SEM micrographs in Figure 4, *e.g.,* (a) and (f), also confirm the presence of molten alloy at very low temperatures prior to their cooling to room-temperature post-experiments, as predicted in Figure 3.

The deposited materials were also characterized by XRD to show their phase assemblies. The examples of the diffractograms are shown in Figure 6. The XRD data show well-crystallized arsenic oxide and metal but perhaps the arsenic sulfides solidified in a glassy form,[33]

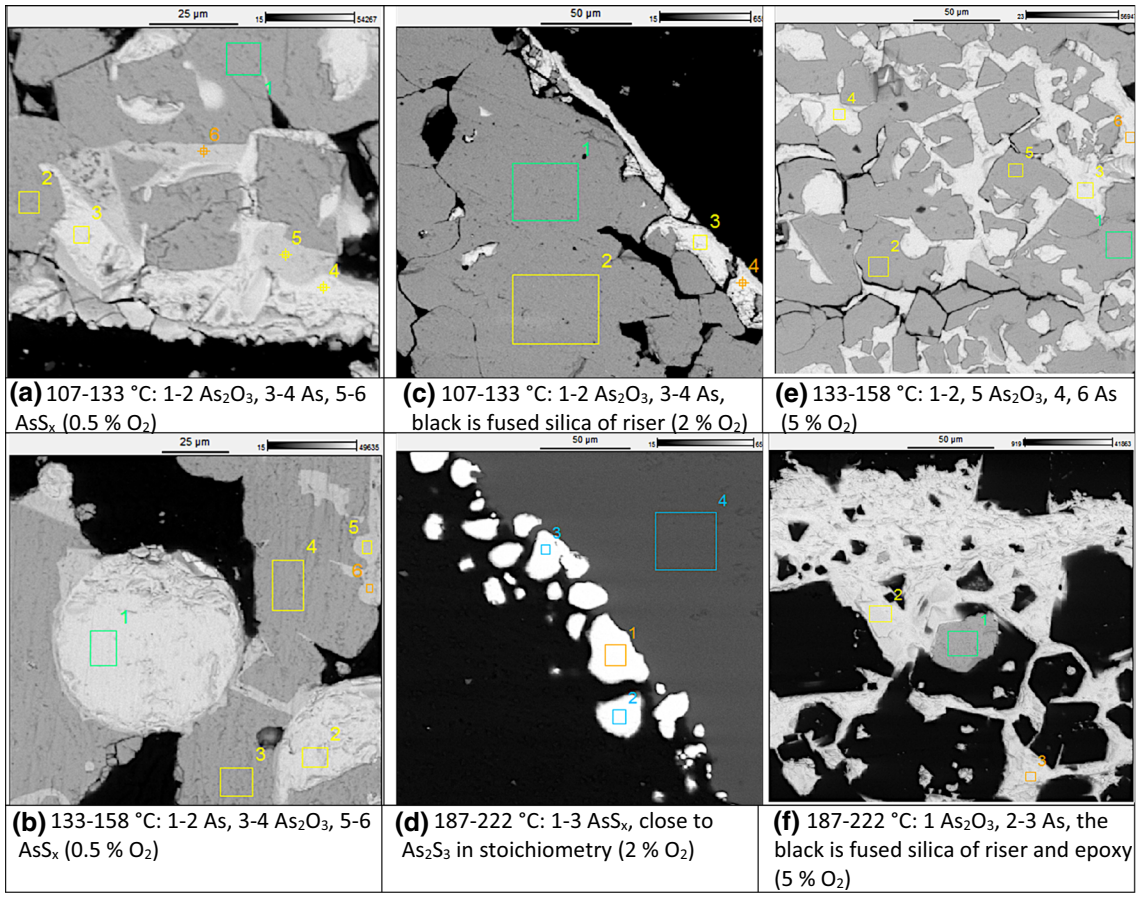

Fig. 5—Cross sections of deposits formed in 0.5, 2 and 5 pct O_2 + 50 pct SO_2 atmospheres at different temperatures.

and thus, they are not found in the XRD diffractogram. However, the EDS and EPMA data show distinct sulfide areas with relative narrow stoichiometries for the metal phase as well as for the sulfides. The average compositions (EDS) of metal, oxide, and sulfide phases were collected in Table S-II in electronic supplementary file. Based on these observations, we can conclude that there has occurred systematic segregation during cooling and solidification of the deposit post-experiments. The EPMA data confirmed the phase compositions obtained by EDS, see Tables S-II and S-III in electronic supplementary file.

As also shown in Figure 6, the amorphous or glassy character of the deposit becomes evident at high temperatures when the baseline of the X-ray diffractogram of the 187 °C to 239 °C sample is diffused and shows much wider peaks than at other temperatures. The solidification, the phase diagram presented above, and the present observations are in good agreement with the conclusions by Kong *et al.*[34] on the sulfur-rich side of the As-O-S system, *i.e.,* As_2O_3-As_2S_3-S sub-ternary in the molten sulfur corner, at 170 °C.

The XPS observations indicate the presence of metallic arsenic (As°), trivalent oxidic and sulfidic, and pentavalent arsenic in deposits. The locations of the peaks exist on lower binding energies than reported for the crystalline phases,[35,36] as shown in Figure 7. Also, the HR spectra recorded from 0.5 vol pct O_2 atmosphere deposits at low temperatures were unstable and degraded so that the obtained peaks were not reproducible when exposed to X-rays in vacuum (or light) for different periods of time.[22,35] Some S 2p spectra also indicated the presence of sulfate in addition to sulfidic and elemental sulfur, see Figure 7(b). The actual form of sulfate is, however, unknown in the absence of hydrogen in the experimental gas mixture, but it may adsorb sulfur trioxide forming sulfuric acid in the sample preparation prior to XPS measurements. The fitted As, O, and S peaks after 10 min total exposure to X-rays have been included Table S-IV, and Figure S-2 (a) through (l) in electronic supplementary file. These XPS analyses confirm the EDS, EPMA, and XRD observations of this study and supplement the speciation by confirming a minor fraction of As(V) to be present in the deposit.

No attempts were made for fitting the oxygen O 1s envelopes with synthetic components. It was also obvious that several deposits reproduced S 2p HR spectra with low S:N ratio which made their fitting unreliable.

The XPS data agree very well with the mineralogical and XRD observations as well as complement the detailed *in situ* phase compositions determined with the EDS and EPMA techniques. It also confirms the

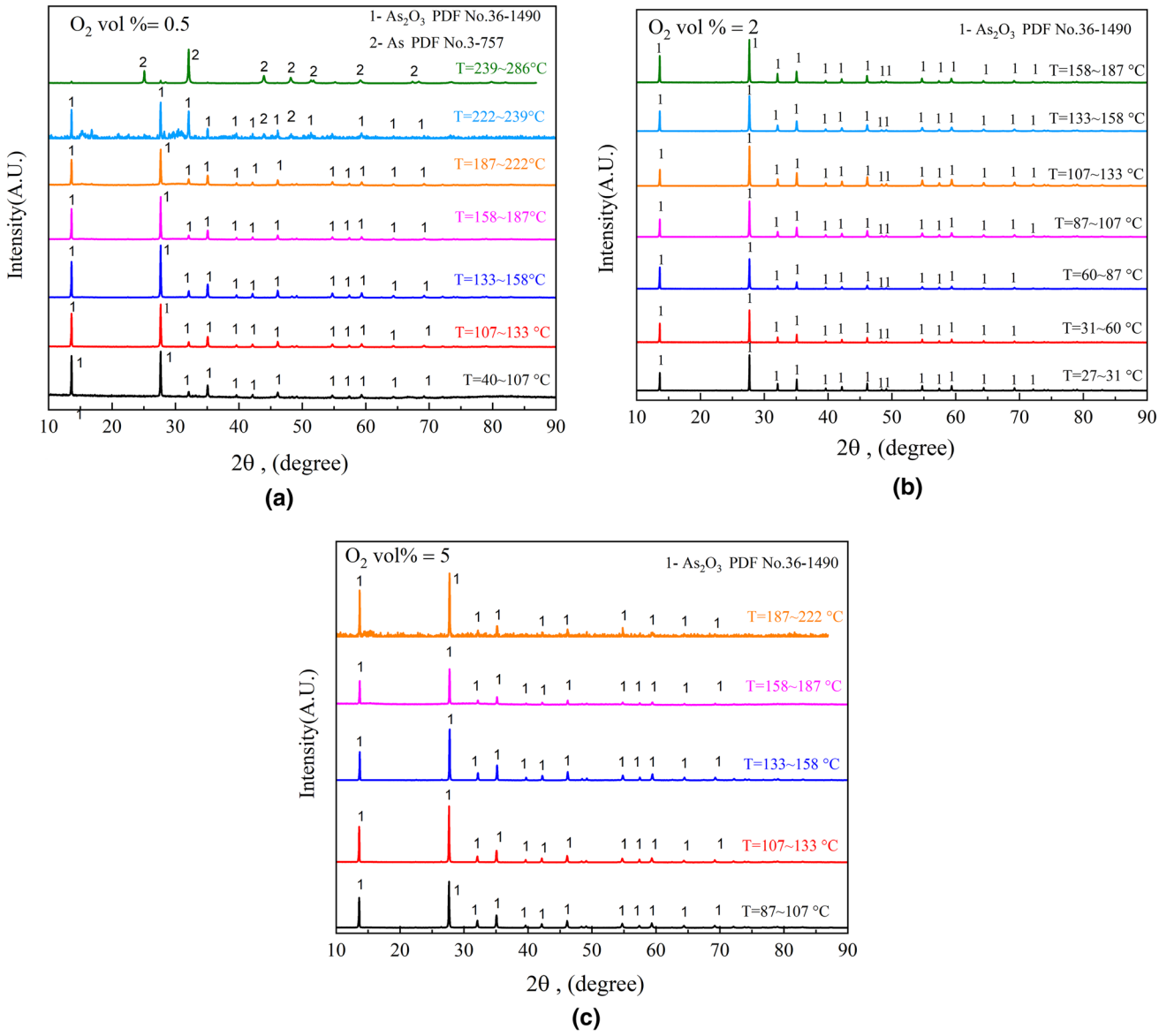

Fig. 6—The XRD spectra obtained from the deposits formed in flowing 0.5, 2, and 5 vol pct O_2-50 vol pct SO_2-N_2 in different temperature zones in the riser tube.

presence of all oxidation degrees of arsenic in the deposits from elemental As to pentavalent As^{5+} in the presence of AsS_x.

IV. DISCUSSION

In combustion engineering, it is well known that arsenic in the feed materials can be trapped from the off-gas by adding suitable additives in the off-gas train,[37,38] ,such as CaO at temperatures of 800 °C to 1000 °C.[38,39] In many studies this depletion process is described as an oxidation sequence between gaseous As_4O_{10}(g), oxygen, and the absorbent forming compounds of pentavalent arsenic *i.e.,* arsenates which also have been identified in the flue dust of sulfide smelters.[9]

In several studies dealing with sulfide smelting, the predominant form of arsenic in smelter flue dusts has been analyzed to be pentavalent arsenic oxide[10,11] even if some authors contradictorily also claim metallic or sulfidic arsenic being present in the industrial WHB, ESP, and stack dusts[9,40] as well as in laboratory-scale experiments.[41] The deposit chemistries in present flue dust-free conditions of this study are summarized in Figure 8.

The present observations indicate clearly how kinetic features, such as nucleation and nucleus growth of arsenic and its compounds, play a crucial role in the precipitation of arsenic compounds at low temperatures below about 350 °C, making possible the formation of lower arsenic oxides and even arsenic metal. Therefore, no major differences were found between different

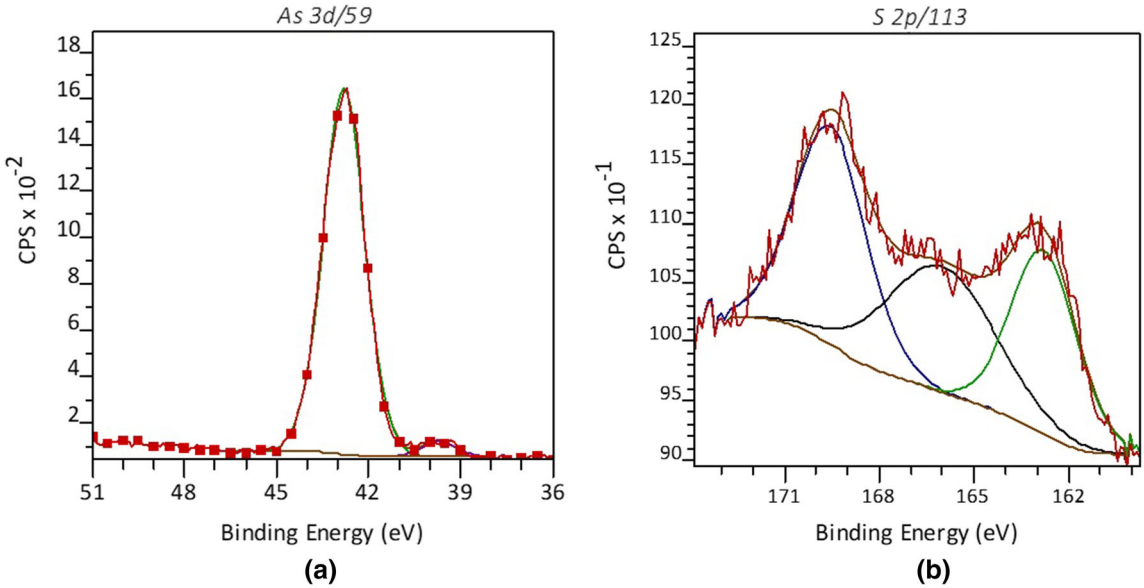

Fig. 7—A fitted HR XPS spectrum of (*a*) As 3d components of metallic and sulfidic arsenic and (*b*) S 2p envelope with sulfidic, elemental, and sulfate components (samples #7 and #DEF, respectively).

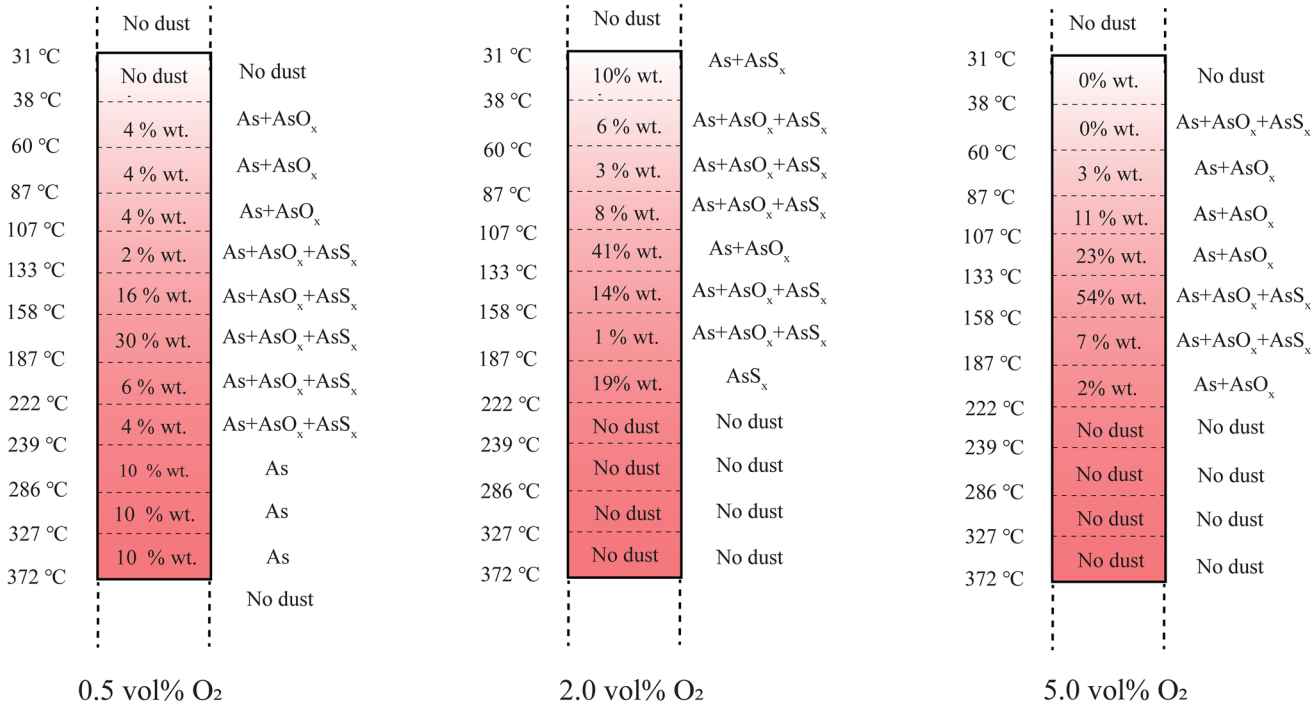

Fig. 8—A schematic pattern of the phases and their mass distributions detected in the deposits at different temperatures and gas mixtures; it is characteristic that metallic arsenic was present at most temperatures in the deposits.

oxygen partial pressures in the deposit mineralogy even if the fractions of metallic arsenic, arsenic sulfides, and arsenic oxides varied as a function of temperature. The most obvious reaction reducing gaseous arsenic oxides is based on the high stability of $SO_3(g)$ at the deposition temperatures, see *e.g.,* Taskinen and Jokilaakso.[2] . The key reaction forming metallic arsenic in the present atmosphere can be written as follows:

$$10SO_2(g) + As_4O_{10}(g) = 4As(s) + 10SO_3(g), \quad [1]$$

where the predominant gaseous arsenic oxide species is taken as an example of the speciation of arsenic oxide in the gas phase.[42,43] The mechanism is analogous to the reduction of selenium oxide vapors by $SO_2(g)$ in the selenium roasting of copper anode slimes[44] used industrially. The formation of arsenic oxide is a

straightforward reduction process of $As_4O_{10}(g)$ to $As_2O_3(s)$ during deposition as follows:

$$4SO_2(g) + As_4O_{10}(g) = 2As_2O_3(s) + 4SO_3(g), \quad [2]$$

but the formation of AsS_x needs more complex interactions between the gas and condensed phases. It is possible only when sulfur undergoes a disproportionation which may be written as follows:

$$As + (2 + x)SO_2(g) = AsS_x + 2SO_{2+x}(g). \quad [3]$$

An important physical feature in the solidification of As-O-S alloys is the very low viscosity of the As-S melts which at the present, temperature range is of the order of magnitude of that of water at 25 °C.[33] The small fraction of silver as impurity in the present deposits (<0.01 wt pct) does not have an impact on the crystallization behavior of the As-S alloys compared to silver-free systems.[45] Thus, this kind of nucleation and precipitation behavior as found in the present study is evidently taking place in the ESP conditions in the sulfide smelting off-gas trains where arsenic oxide precipitation occurs in low-flue dust environments. In the present experimental conditions, the speciation of arsenic above 250 °C was, however, unknown and the presence of equilibrium conditions for arsenic and the other gaseous species cannot be assured.

The observed structures of the deposit are in a good agreement with the findings by Riley *et al.*[46] in oxygen-free systems. The silica detected in the deposits is a result of the very high adhesion between As-S glasses and SiO_2.[47]

The present experimental temperature range represents typical values for the sulfide smelter off-gas post waste heat boiler (WHB), in the electrostatic precipitator (ESP). Most flue dust components have been settled and removed from the off-gas in WHB.[6] Therefore, this study represents a good estimate and description of the arsenic precipitation processes in ESP and post it in the off-gas train. The speciation of arsenic in the industrial sulfide smelter flue dusts indicates the presence of arsenates, typically those of copper and iron,[48] formed by gas-solid reactions in the WHB at temperatures >350 °C.

V. CONCLUSIONS

This study explains the disagreements in many industrial observations on the sulfide smelting flue dust chemistries, which may rise from, *e.g.,* minor undocumented differences in the process conditions and sample treatment as well as delays before analyses outside the gas train. The mechanism of arsenic vapor nucleation and precipitation in O_2- and SO_2-bearing atmospheres, whether there is a high or low sulfur dioxide concentration in the atmosphere, is a complex phase conversion controlled by chemical reactions between the arsenic species in the atmosphere and the strong tendency of generating $SO_3(g)$ at low temperatures. Thus, there are very few possibilities in interacting with and controlling the chemistry when arsenic vapors condense in the off-gas train of the industrial sulfide smelters.

The present novel data generated experimentally clearly reveal the kinetically constrained formation mechanism of the arsenic-containing deposits differing from the thermodynamic equilibrium compositions corresponding to these temperatures and gas atmospheres. The SEM-EDS, EPMA, XRD, and XPS analyses supplement each other and are in good agreement. Within the experimental range studied, it was observed that decreasing volumetric concentration of oxygen in the gas atmosphere increased the upper temperature of the deposit formation and favored metallic arsenic deposit. Specifically, the highest extent of elemental arsenic deposition was observed at around 250-350 °C, with 0.5 vol pct oxygen in the gas. On the other hand, deposition of the oxide and sulfide species occurred at lower temperatures, mainly below 200 °C, while the phase fraction of As_2O_3 is major in most deposits collected. Therefore, careful handling of the industrial FSF and FCF off-gas and controlling oxygen concentration to the preferred level is a possibility to control the deposits chemistry. However, the deposit chemistry is more complex in the industrial case with base metal dust particles present.

ACKNOWLEDGMENTS

We used the experimental resources provided by the RAMI Infrastructure (Raw Materials Finland) housed by Aalto University, GTK and VTT. Ms Miao Tian is kindly acknowledged for her assistance in XRD measurements, Ms Fabiola Lasar in experimental part and Dr Jouko Lahtinen for the XPS measurements. Funding from Tocanem program (Business Finland; Grant #2118452) is greatly appreciated.

FUNDING

Open Access funding provided by Aalto University.

CONFLICT OF INTEREST

On behalf of all authors, the corresponding author states that there is no conflict of interest.

SUPPLEMENTARY INFORMATION

The online version contains supplementary material available at https://doi.org/10.1007/s11663-023-02871-9.

REFERENCES

1. F.R.A. Jorgensen and P.T.L. Koh: *JOM*, 2001, vol. 53(5), pp. 16–20.
2. P. Taskinen and A. Jokilaakso: *Metall. Mater. Trans. B*, 2021, vol. 52B(5), pp. 3524–42.
3. N.E. Tuffrey, G.G. Richards, and J.K. Brimacombe: *Metall Mater. Trans. B*, 1995, vol. 26B(5), pp. 929–42.
4. T. Laurila, R. Hernberg, R. Oikari, T. Joutsenoja, P. Mikkola, T. Ranki-Kilpinen, and P. Taskinen: *Metall Mater. Trans. B*, 2005, vol. 36B(2), pp. 201–08.
5. Kojo I., Lahtinen M., and Miettinen E.: Flash Converting – Sustainable Technology Now and in the Future. In: Internat. Peirce-Smith Converting Centennial (Ed. J. Kapusta and T. Warner). TMS, Warrendale (PA), 2009, pp. 383–95.
6. Y. Yang, A. Jokilaakso, P. Taskinen, and M. Kytö: *JOM*, 1999, vol. 51(5), pp. 36–40.
7. J. Yli-Penttilä, E. Peuraniemi, A. Jokilaakso, and K. Riihilahti: *Miner. Metall. Process.*, 1998, vol. 15(4), pp. 41–47.
8. H. Henao, I. Paredes, R. Diaz, and J. Ortiz: *J. Miner. Mater. Charact. Eng.*, 2021, vol. 9, pp. 609–20.
9. Y. Chen, Z. Zhao, P. Taskinen, Y. Liang, H. Ouyang, B. Peng, A. Jokilaakso, S. Zhou, T. Chen, N. Peng, and H. Liu: *Metall. Mater. Trans. B*, 2020, vol. 51B(6), pp. 2596–2608.
10. H. Zhou, G. Liu, L. Zhang, and C. Zhou: *Chem. Eng. J.*, 2021, vol. 423, p. 130193.
11. H. Zhou, G. Liu, L. Zhang, C. Zhou, M.M. Mian, and A.I. Cheema: *Environ. Poll.*, 2021, vol. 270, p. 116203.
12. M. Moats, L. Alagha, and K. Awuah-Offei: *J. Clean. Product*, 2021, vol. 307, p. 127207.
13. E. Klaffenbach, S. Mostaghel, M. Guo, and B. Blanpain: *J. Sustain. Metall.*, 2021, vol. 7(2), pp. 664–83.
14. L. Reijnders: *Miner. Process. Extract Metall. Rev.*, 2022, vol. 43(8), pp. 1021–48.
15. D. Shishin, T. Hidayat, J. Chen, P.C. Hayes, and E. Jak: *J. Chem. Thermodyn.*, 2019, vol. 135, pp. 175–82.
16. S. Sineva, M. Shevchenko, D. Shishin, T. Hidayat, J. Chen, P.C. Hayes, and E. Jak: *JOM*, 2020, vol. 72(10), pp. 3401–09.
17. A. Lisak and K. Fitzner: *J. Phase Equilib.*, 1994, vol. 15(2), pp. 151–54.
18. Brunetti B., Piacente V., and Scardala P.: J. Chem. Eng. Data, 2007, vol. 52 (4), pp. 1343-1346.
19. Taskinen P., Vartiainen A., and Jokilaakso A.: Thermochemical description of antimony and arsenic in the suspension stage of the Outokumpu Flash Smelting Furnace. In: H.H Kellogg Int. Symp. (N. Themelis & P. Duby, Eds). TMS, Warrendale (PA), 1991, pp. 45-67.
20. K. Wegner, B. Walker, S. Tsantilis, and S.E. Pratsinis: *Chem. Eng. Sci.*, 2002, vol. 57(10), pp. 1753–62.
21. E. Karlsson, J. Neuhausen, R. Eichler, A. Aerts, I.I. Danilov, A. Vögele, and A. Türler: *J. Radioanal. Nucl. Chem.*, 2020, vol. 326(2), pp. 1249–58.
22. H. Viltres, O.F. Odio, L. Lartundo-Rojas, and E. Reguera: *Appl. Surf. Sci.*, 2020, vol. 511, p. 145606.
23. CasaXPS Manual, vers 2.3.15 (rev 1.0). Casa Software Ltd., UK, 2009.
24. G.H. Major, N. Fairley, P.M.A. Sherwood, M.R. Linford, J. Terry, V. Fernandez, and K. Artyushkova: *J. Vac. Sci. Technol. A*, 2020, vol. 38, p. 0612013.
25. C.I. Corkhill and D.J. Vaughan: *Appl. Geochem.*, 2009, vol. 24(12), pp. 2342–61.
26. H.A. Bullen, M.J. Dorko, J.K. Oman, and S.J. Garrett: *Surf. Sci.*, 2003, vol. 531, pp. 319–28.
27. M. Fantauzzi, B. Elsener, D. Atzei, A. Rigoldi, and A. Rossi: *RSC Adv.*, 2015, vol. 5, p. 75953.
28. Fleet M.E., Chryssoulis S-L., MacLean P.J., Davidson R., and Weisener C.G.: Canad. Mineral., 1993, vol. 31, pp. 1-17.
29. M.E. Hirsch, R.O. Sterling, F.E. Huggins, and J.J. Helble: *Environ. Eng. Sci.*, 2000, vol. 17(6), pp. 315–27.
30. V. Prostakova, D. Shishin, and E. Jak: *Calphad*, 2021, vol. 72, p. 102235.
31. Gisby J.: Phase Equilibria Data for Oxide, Sulphide and Fluoride System. Project RC254 (Progress Note 6). NPL Report MAT (RES) 268, National Physical Laboratory, Teddington (UK), 2016, 149 p.
32. R.C. Paule and J. Mandel: *Pure Appl. Chem.*, 1972, vol. 31(3), pp. 395–431.
33. I.V. Skripachev, M. El-Amraoui, Y. Messaddeq, and S.H. Santagneli: *Int. J. Appl. Glass. Sci.*, 2013, vol. 4(3), pp. 256–65.
34. L. Kong, Z. Xia, X. Hu, and X. Peng: *J. Hazard. Mater.*, 2021, vol. 419, p. 126390.
35. A. Kovalskiy, J.R. Neilson, A.C. Miller, F.C. Miller, M. Vleck, and H. Jain: *Thin Solid Films*, 2008, vol. 516(21), pp. 7511–18.
36. R. Golovchak, O. Shpotyuk, J.S. Mccloy, B.J. Riley, C.F. Windisch, S.K. Sundaram, A. Kovalskiy, and H. Jain: *Philos. Mag.*, 2010, vol. 90(34), pp. 4489–4501.
37. C. Tian, R. Gupta, Y. Zhao, and J. Zhang: *ACS Energy Fuels*, 2016, vol. 30(8), pp. 6201–09.
38. B. Song, K. Yuan, Y. Wei, D. Chen, F. Meng, Q. Cao, M. Song, and H. Liu: *ACS Eviron. Sci. Technol.*, 2021, vol. 55(13), pp. 8613–21.
39. S. Yu, C. Zhang, L. Ma, P. Tan, Q. Fang, and G. Chen: *J. Hazard. Mater.*, 2021, vol. 403, p. 123617.
40. J.M. Skeaff, Y. Thibault, and D.J. Hardy: *Environ. Monit. Assess.*, 2011, vol. 177(1), pp. 165–92.
41. P.N. Prasad, A. Lennartsson, and C. Samuelsson: *Metall. Mater. Trans. B*, 2021, vol. 52B(3), pp. 1866–85.
42. G.S. Pokrovski, I.V. Zakirov, J. Roux, D. Testemale, J. Hazelmann, AYu. Bychkov, and G.V. Golikova: *Geochim. Cosmochim. Acta*, 2002, vol. 66(19), pp. 3453–80.
43. S.M. Sadegh, J.D. Miller, and H.H. Huang: *Metall. Res. Technol.*, 2014, vol. 111(2), pp. 95–105.
44. O. Hyvärinen, L. Lindroos, and E. Yllö: *JOM*, 1989, vol. 41(7), pp. 42–43.
45. E. Bychkov, D.J. Price, and A. Lapp: *J. Non-Cryst. Solids*, 2001, vol. 293–295, pp. 211–19.
46. B.J. Riley, B.R. Johnson, S.K. Sundaram, M.H. Engelhard, R.E. Williford, and J.D. Olmstead: *Phys. Chem. Glasses*, 2006, vol. 47(6), pp. 675–80.
47. M.F. Churbanov, S.V. Mishinov, V.S. Shiryaev, and L.A. Ketkova: *J. Non-Cryst. Solids*, 2018, vol. 480, pp. 3–7.
48. Y. Chen, S. Zhu, P. Taskinen, N. Peng, B. Peng, A. Jokilaakso, H. Liu, Y. Liang, Z. Zhao, and Z. Wang: *Miner. Eng.*, 2021, vol. 164, p. 106796.